Tunneling Spectroscopy of Quantum Spin Liquids

Elio J. König,[1] Mallika T. Randeria,[2] and Berthold Jäck[3]
[1]Department of Physics and Astronomy, Center for Materials Theory, Rutgers University, Piscataway, New Jersey 08854, USA
[2]Department of Physics, Massachusetts Institute of Technology, Cambridge, Massachusetts 02139, USA
[3]Princeton University, Joseph Henry Laboratory at the Department of Physics, Princeton, New Jersey 08544, USA

(Received 21 August 2020; accepted 4 December 2020; published 31 December 2020)

We examine the spectroscopic signatures of tunneling through a Kitaev quantum spin liquid (QSL) barrier in a number of experimentally relevant geometries. We combine contributions from elastic and inelastic tunneling processes and find that spin-flip scattering at the itinerant spinon modes gives rise to a gapped contribution to the tunneling conductance spectrum. We address the spectral modifications that arise in a magnetic field, which is applied to drive the candidate material α-$RuCl_3$ into a QSL phase, and we propose a lateral 1D tunnel junction as a viable setup in this regime. The characteristic spin gap is an unambiguous signature of the fractionalized QSL excitations, distinguishing it from magnons or phonons. We discuss the generalization of our results to a wide variety of QSLs with gapped and gapless spin correlators.

DOI: 10.1103/PhysRevLett.125.267206

Introduction.—Geometric frustration of localized spins can suppress magnetic order and favor the formation of a quantum spin liquid (QSL) state, which is characterized by a macroscopic ground state of entangled quantum spins with absent long-range order [1]. The spin degree of freedom of a QSL state can fractionalize into a set of anyonic excitations, where the exactly solvable Kitaev model on a honeycomb lattice predicts the emergence of localized, gapped $\mathbb{Z}_2$ fluxes and an itinerant, relativistic Majorana spinon mode [2]. When time reversal symmetry is broken, e.g., by a magnetic field, the bulk spinon spectrum is further expected to acquire a topological mass gap, giving rise to emergent 1D chiral Majorana edge modes. Their non-Abelian quantum statistics could present avenues for implementing topologically protected quantum computation [3], whose prospect promotes today's intense research efforts on this topic [4–7].

Experimental evidence for these emergent quasiparticles is rare [8–11]. The search for material realizations of the Kitaev model has focused on Mott-Hubbard systems with partially filled t_{2g} levels and strong spin-orbit coupling [4]. Examples encompass the iridates with effective spin-1/2 moments on a honeycomb lattice and bond directional Kitaev interactions. While many of these compounds were found to exhibit long-range magnetic order [12], hydrogen intercalation appears to stabilize a QSL [13]. The layered transition-metal trihalide α-$RuCl_3$ [14], with similar properties to those of the iridates, has been gaining traction as a candidate Kitaev QSL material. Most prominently, recent results from neutron scattering on this compound suggest a magnetically disordered state [15,16], consistent with the observation of a half-integer thermal quantum Hall effect at finite magnetic fields [17]—a telltale sign of a chiral Majorana boundary mode [2]. Nevertheless, the chargeless character of these emergent quasiparticles and the electrically insulating nature of QSL limit the range of suitable measurement techniques and, in

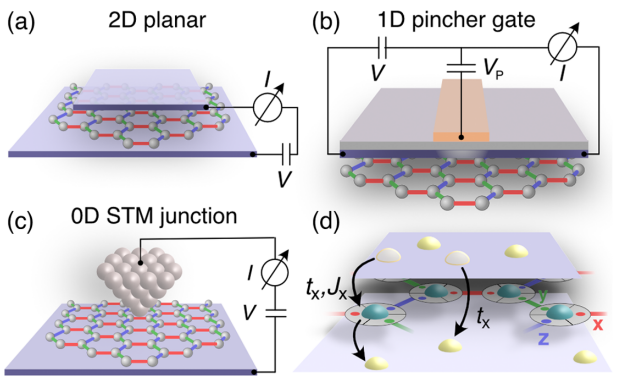

FIG. 1. (a) 2D planar tunnel device geometry; a single- or few-layer QSL material is sandwiched between two metallic 2D electrodes, e.g., graphene [19,23]. The tunnel current I measured as a function of the applied bias voltage V provides insight on the contributing tunnel processes. (b) 1D pincher gate geometry; a lateral 1D tunnel junction geometry can be created on top of a QSL bulk crystal. A pincher gate can induce an electrically insulating region in a suitable electrode material, e.g., bilayer graphene [25] with a displacement field, by applying a voltage V_P to serve as a 1D tunnel barrier. (c) Zero-dimensional tunnel junction between an STM tip and an electrically conducting substrate, which supports a monolayer QSL material on its surface. (d) Illustration of the relevant tunnel processes in a M-QSL-M geometry. The electron can tunnel either elastically with amplitude t_x or inelastically with amplitude J_x, undergoing spin-flip scattering at the fractionalized spin degree of freedom of the QSL.

particular, render their detection in electrical transport measurements challenging [18].

Previous experiments in planar junctions made from exfoliated 2D materials established a new means to investigate atomically thin magnetic insulators, by using them as tunnel barriers between two graphite electrodes [19,20]. Considering the electrically insulating behavior of QSL materials, this concept can be naturally extended to probe their charge-neutral quasiparticle excitations. The tunneling electron can undergo inelastic spin scattering at the fractionalized spin states of the QSL, potentially leaving distinct spectroscopic fingerprints in its tunneling characteristics, while its charge degree of freedom participates only in the creation of electron-hole pairs at the electrodes. From a practical perspective, the QSL candidate α-$RuCl_3$ can be exfoliated into the monolayer limit [21,22] and offers direct avenues to explore inelastic spin scattering at the Majorana spinon mode in similar planar device structures [23]. However, little is known about the influence of the tunnel junction geometry, the electronic properties of the metallic leads on this inelastic spin scattering and, most importantly, under which circumstances this process produces a signal strong enough to be detected in an experiment.

In this Letter, we methodologically investigate the general spectroscopic tunneling characteristics of M-QSL-M tunnel junctions, which are formed between two metallic electrodes (M) separated by a thin, electrically insulating QSL barrier, in different experimentally relevant geometries [Figs. 1(a)–1(c)]. For our theoretical analysis, we consider a single-layer Kitaev QSL as the tunnel barrier and develop the full dc and ac bias voltage-dependent tunnel conductance expressions, including both scalar and spin-flip contributions, as a function of the QSL spin structure factors [24]. For all investigated junction geometries, we find that spin-flip scattering at gapless Majorana spinon modes yields unique features in the electron tunneling spectra that can be detected in experiments.

Model.—A simple physical model to describe the M-QSL-M junctions presented in Fig. 1 is given by $H = H_{\text{leads}} + H_{\text{tun}} + H_{\text{QSL}}$, where

$$H_{\text{leads}} = \sum_{\xi=1,2} \sum_{\sigma} \int \frac{d^2k}{(2\pi)^2} c^{\dagger}_{\mathbf{k},\sigma,\xi} [\epsilon(\mathbf{k}) - \mu] c_{\mathbf{k},\sigma,\xi}, \tag{1a}$$

$$H_{\text{tun}} = \sum_{\mathbf{x}} \sum_{\sigma,\sigma'} [t_{\mathbf{x}} \delta_{\sigma\sigma'} + J_{\mathbf{x}} \vec{\sigma}_{\sigma,\sigma'} \cdot \hat{\vec{S}}(\mathbf{x})] \; [c^{\dagger}_{\mathbf{x}1\sigma} c_{\mathbf{x}2\sigma'} e^{ieVt} + \text{H.c.}]. \tag{1b}$$

H_{leads} describes the leads, H_{tun} the tunnel process, and H_{QSL} the QSL serving as the tunnel barrier. The index $\xi = 1, 2$ labels the leads, $\mathbf{x}$ runs over the lattice sites of the quantum magnet, $\hat{\vec{S}}(\mathbf{x})$ is the spin operator of the QSL at site $\mathbf{x}$, and $\vec{\sigma}$ denotes the spin of the tunneling electron. The first (second) term $t_{\mathbf{x}}$ ($J_{\mathbf{x}}$) in the tunneling matrix elements stems from electrons passing through the QSL without affecting the spin configuration (while creating a spin flip) at site $\mathbf{x}$ [Fig. 1(d)]. When the QSL material is placed on a metallic substrate, one may also expect Kondo-like spin-spin interactions with the electron in the underlying metals. We neglect such interactions, because the vison gap in Kitaev materials prevents a weak coupling Kondo effect [26,27].

Here, we study three experimental setups: First, we study planar 2D to 2D tunneling $t_{\mathbf{x}} = t_0, J_{\mathbf{x}} = J_0$ across the M-QSL-M junction [Fig. 1(a)]. Second, we study a one-dimensional tunneling constriction $t_{\mathbf{x}} = t_0\delta_{x,0}, J_{\mathbf{x}} = J_0\delta_{x,0}$ [Fig. 1(b)]. Without a magnetic field, this setup corresponds to lateral tunneling between two-dimensional electron gases (2DEGs), but in the presence of a sufficiently strong field it represents tunneling between quantum Hall edge states. Third, we consider a zero-dimensional point contact $t_{\mathbf{x}} = t_0\delta_{\mathbf{x},0}, J_{\mathbf{x}} = J_0\delta_{\mathbf{x},0}$ [Fig. 1(c)], which describes the physics of a classic scanning tunneling microscope (STM) experiment.

As the physical process of tunneling through a Mott-insulating material involves the virtual double occupancy of sites, superexchange generically leads to [28] $J_{\mathbf{x}} \sim t_{\mathbf{x}} \sim V^2/U$, where V is the hybridization between the conduction electrons of the leads and the localized electrons in the QSL and U is the Mott-Hubbard gap of the latter. Hence, the elastic and inelastic tunnel probabilities are of comparable magnitude: $t_{\mathbf{x}}/J_{\mathbf{x}} \sim 1$. In the case of the 1D tunneling barrier [Fig. 1(b)], $t_{\mathbf{x}}$ may, however, acquire an additional contribution from direct tunneling between the leads, in which case $|t_{\mathbf{x}}| \gg |J_{\mathbf{x}}|$.

For the analytical study of tunneling through a QSL state, we mostly focus on the case of the exactly solvable Kitaev model [2] in the isotropic limit; in this case,

$$H_{\text{QSL}} = K \sum_{i=x,y,z} \sum_{\langle \mathbf{x},\mathbf{x}' \rangle_i} \hat{S}_i(\mathbf{x}) \hat{S}_i(\mathbf{x}'). \tag{1c}$$

The interactions of the Kitaev model K are bond-directed Ising interactions, as displayed in Fig. 1(d).

We conclude this section by listing the assumptions behind our calculations: We consider the limit when the Fermi wavelength λ_F of the metallic leads exceeds the lattice constant a of the magnet such that a continuum treatment of the leads is justified. Except the case of the STM tip electrode in Fig. 1(c), it is furthermore important that the leads are strictly two dimensional, as realized in graphene-based experimental setups [19]. Finally, we disregard umklapp scattering in the section on planar tunneling, which is a good approximation when the unit cell of the magnet equals or exceeds the unit cell of the materials at the leads (this is the case, e.g., for α-$RuCl_3$ and graphene [37]).

Tunneling current.—The leading-order tunneling current $I = I^{\mathrm{el}} + I^{\mathrm{inel}}$ is given by contributions from elastic (I^{el}) and inelastic (I^{inel}) tunneling processes, respectively. The first contribution to the current reflects the standard tunnel current across the junction:

$$I^{\mathrm{el}} = 2\pi \frac{e}{h} \sum_{\mathbf{x},\mathbf{x}'} t_{\mathbf{x}} t_{\mathbf{x}'} [\mathcal{A}^{1^\dagger 2}_{\mathbf{x},\mathbf{x}'}(eV) - 1 \leftrightarrow 2]. \tag{2a}$$

We denote the spectral weight of a particle-hole pair with a particle (hole) in electrode 1 (electrode 2) by $\mathcal{A}^{1^\dagger 2}_{\mathbf{x},\mathbf{x}'}(E)$, where $E = eV$ is the energy and V is the bias voltage across the junction. The current presented in Eq. (2a) can be interpreted as a difference of Fermi golden rule rates, where the matrix element is encoded in the spatial dependence of $t_{\mathbf{x}}, \mathcal{A}^{1^\dagger 2}_{\mathbf{x},\mathbf{x}'}(E)$.

We now address the inelastic contribution to the tunnel current, which can be expressed as [38,39]

$$I^{\mathrm{inel}} = \frac{e}{h} \sum_{\mathbf{x},\mathbf{x}'} \int dE J_{\mathbf{x}} J_{\mathbf{x}'} \{\mathcal{A}^{\mathrm{spin}}_{\mathbf{x},\mathbf{x}'}(eV - E) \mathcal{A}^{1^\dagger 2}_{\mathbf{x},\mathbf{x}'}(E) \times [n(eV - E) - n(E)] - 1 \leftrightarrow 2\}. \tag{2b}$$

Analogously to Eq. (2a), the inelastic current is generated by the creation of particle-hole pairs with charges on opposite sides of the junction. In contrast to the scalar contribution, I^{inel} corresponds to inelastic scattering: The electrons deposit energy into the spin system during the tunneling process (both spin-conserving and spin-flip processes are included). This amplitude is weighted by the difference in occupation of the spin and particle-hole modes [$n(E)$ is the Bose-Einstein distribution] and, most importantly, by the spectral weight of the spin excitations $\mathcal{A}^{\mathrm{spin}}_{\mathbf{x},\mathbf{x}'}(E) = -2\mathrm{Im}C^+(\mathbf{x},\mathbf{x}';E)$, where

$$C^+(\mathbf{x},\mathbf{x}';t,t') = -i\theta(t-t') \sum_{i=x,y,z} \langle [\hat{S}_i(\mathbf{x},t), \hat{S}_i(\mathbf{x}',t')] \rangle. \tag{3}$$

In the following, we focus on QSLs in which the retarded spin susceptibility $C^+(\mathbf{x},\mathbf{x}';t,t') = C^+(\mathbf{x}-\mathbf{x}';t-t')$ decays at least exponentially in space. This applies to gapped QSLs as well as to the integrable Kitaev model. When the correlation length is small as compared to the Fermi wavelength, the inelastic contribution to the differential tunnel conductance dI^{inel}/dV at zero temperature can, therefore, be simplified to [28]

$$\frac{dI^{\mathrm{inel}}}{dV} = -G_0 \sum_{\mathbf{x},\mathbf{x}'} \frac{J_{\mathbf{x}} J_{\mathbf{x}'}}{t_0^2} \int_0^{\mathrm{eV}} \frac{dE}{2\pi} \mathrm{Im}C^+(\mathbf{x}-\mathbf{x}';E). \tag{4}$$

Here, $G_0 \propto t_0^2$ is the dimensionless conductance of a point contact [28]. The integral in Eq. (4) is largely independent of the tunnel junction geometry, and it can be evaluated on the basis of the short-ranged spin correlator $\mathrm{Im}C^+(\mathbf{x},\mathbf{x}';E)$.

In the specific case of the Kitaev spin liquid, where $\mathrm{Im}C^+(\mathbf{x},\mathbf{x}';E)$ can be derived analytically [24,28,29], only on-site and nearest-neighbor correlators are nonzero [29] [Fig. 2(a)]. The gap $\sim 0.26\,K$ in the spectrum is a manifestation of absent spin order, and it results from creating virtual excitations of the $\mathbb{Z}_2$ gauge field ("visons"). Beyond this excitation gap, the continuum of Majorana spinons appears as a broad hump. The prefactor to the integral in Eq. (4) depends on the tunnel-junction geometry,

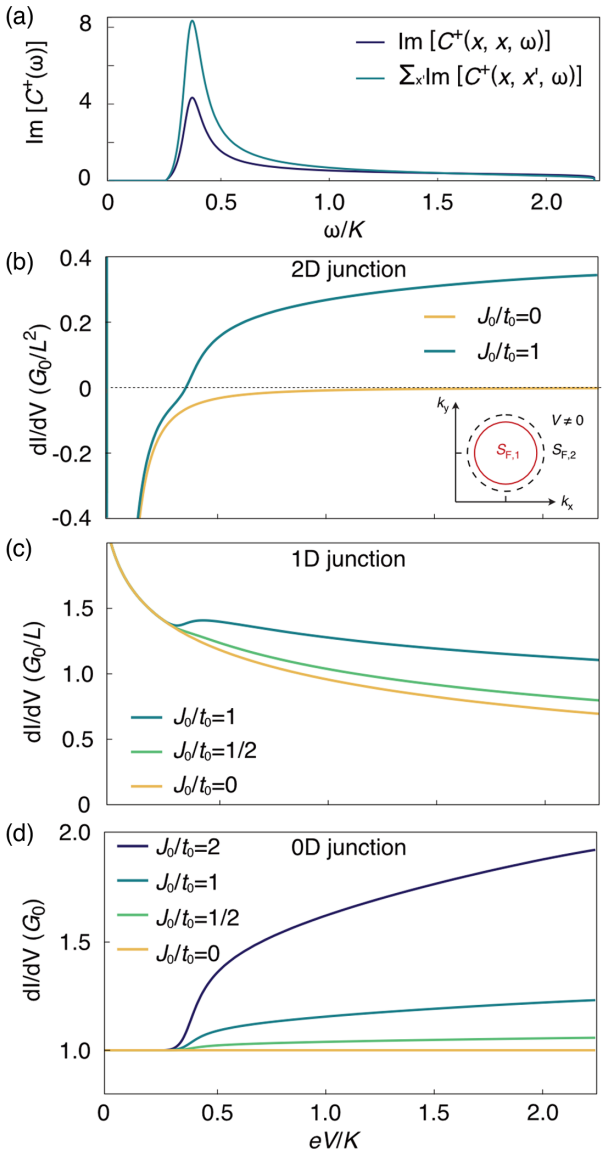

FIG. 2. (a) Short-ranged dynamical spin susceptibility $\mathrm{Im}[C^+(\omega)]$ [24,29] as a function of frequency ω, normalized by the Kitaev interaction K. (b)–(d) Calculated dI/dV spectra for electron tunneling across junctions of different geometries at different J_0/t_0 ratios as a function of the applied bias voltage V. The case of purely elastic electron tunneling corresponds to $J_0/t_0 = 0$. The inset in (b) depicts the mismatch between the Fermi surfaces $S_{F,1}$ and $S_{F,2}$ between the electrode 1 and 2, respectively, at $V \neq 0$.

and it acquires a scaling $\sim L^d$ (L denotes the size and d the dimension of the junction), due to the sum over the mean positions.

We plot the calculated dI/dV spectra in Fig. 2, containing both elastic and inelastic contributions, for the different device geometries in Figs. 1(a)–1(c). These spectra were obtained for $\lambda_F/a = 2\pi$, $E_F/K = 2.5$, and $\Gamma/K = 1/1000$, where E_F (Γ) is the Fermi energy (quasiparticle decay rate), and for different values of the tunnel coupling ratio t_0/J_0 (for other values of E_F/K, see Ref. [28]). In Fig. 2, we present results for the dc tunneling experiment only; yet it bears noting that we obtain qualitatively similar characteristics for the ac tunneling conductance $\mathrm{Re}[G(\Omega)]$ [28], whose properties could be probed using terahertz techniques [40,41].

Discussion of M-QSL-M setups.—The comparison of calculated dI/dV spectra in Figs. 2(b)–2(d) shows that inelastic electron scattering off the itinerant spinon mode yields a gapped finite contribution to the dI/dV spectrum with an onset at $eV \approx 0.26\ K$ (for α-$RuCl_3$, $K \sim 10$ meV [37,42]). A closer inspection, however, reveals that the relative contribution of this inelastic channel to the total tunnel conductance varies significantly between the respective tunnel junction geometries, as we discuss below.

Planar 2D tunnel junctions [23], with metallic 2DEGs as the electrodes [Fig. 1(b)], appear particularly well suited for the investigation of the spin-flip tunneling process. At $J_0/t_0 \neq 0$, I^{inel} contributes a prominent bump with an onset at finite voltage in the dI/dV spectrum. The elastic channel (cf. the curve at $J_0/t_0 = 0$) remains largely suppressed at $V \neq 0$. Owing to the mismatch of Fermi surfaces in the top and bottom electrodes, momentum and energy conservation cannot be fulfilled simultaneously at $V \neq 0$ [cf. the inset in Fig. 2(b)]. Therefore, I^{el}/V is a Lorentzian peak of width Γ, which is centered at $V = 0$, and dI^{el}/dV is small and negative at finite bias voltages [43].

The lateral 1D tunnel junction geometry [Fig. 1(b)] shows fundamentally different dI/dV-spectrum characteristics [Fig. 2(c)]. A benefit of this geometry is the possibility to place the tunnel electrodes directly on the surface of bulk crystals, which likely expands the range of material candidates, as it circumvents challenges related to monolayer exfoliation and unwanted doping [22,44]. However, the dominant logarithmic contribution to the dI/dV spectrum originates from elastic tunneling between the 2DEGs, whereas the contribution from spin-flip tunneling is comparably small.

The third geometry, a 0D tunnel junction, can be formed between an atomically sharp tip of a scanning tunneling microscope and a 2D metallic substrate, which supports the thin QSL material layer [Fig. 1(c)]. Atomic-scale resolution combined with the ability to distinguish spectral features of the surface from the edge has inspired recent proposals to study QSL spinon modes and chiral Majorana edge modes in such STM setups [45,46]. Nevertheless, Fig. 2(d) illustrates that a significant spinon-induced bump on top of the constant dI^{el}/dV spectrum develops only for $J_{\mathbf{x}}/t_{\mathbf{x}} \gtrsim 1$. On the other hand, the continuous tunability of the STM tip-sample distance could serve as a valuable tuning knob to test the evolution of this spectral feature as a function of the STM tunnel junction transparency. Hence, inelastic tunneling with an STM could present an attractive experimental approach, not least in view of the recent advances in epitaxial growth of the non-Kitaev QSL candidate materials 1T-TaS_2 and 1T-$TaSe_2$ [47–52].

Quantum Hall regime.—Up to now, we considered experimental scenarios, in which the electrodes, except for the case of a STM geometry, can be described by a metallic 2DEG. However, in the case of α-$RuCl_3$, a strong out-of-plane magnetic field may be applied to engender the putative QSL state [17] and induce Landau quantization in the 2D electrodes, which has a profound influence on the spectral tunnel characteristics for the 2D and 1D tunnel junction geometry; cf. Figs. 1(a) and 1(b). Previous experiments on 2D planar tunnel junctions show that Landau-level spectra in 2D graphene electrodes results in a complex dI/dV spectrum [19], which presumably renders the observation of tunneling signatures of Majorana spinons [23] challenging.

By contrast, we establish the case of the 1D lateral tunnel junction in the presence of quantum Hall (QH) edge states as a setup which favors the detection of inelastic spin-flip scattering in the dI/dV spectrum [Fig. 3(a)]. In the limit of $K/\omega_c \ll 1$, when the cyclotron frequency ω_c exceeds the Kitaev coupling, tunneling between the chiral edge modes in both junction electrodes [Fig. 3 (inset)] results in a constant tunnel current $I^{\mathrm{el}} \propto G_0 L \mathrm{sgn}(eV)$ [28,30]. Hence,

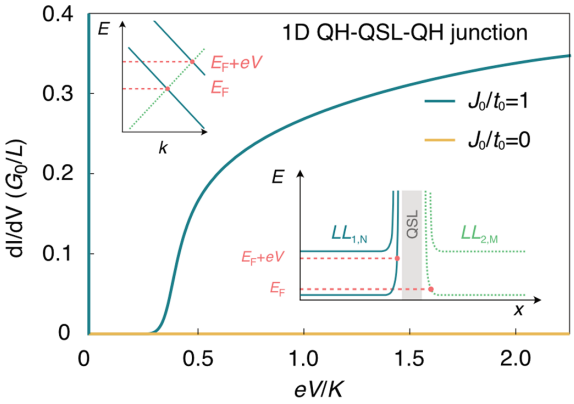

FIG. 3. (a) Calculated dI/dV spectrum for electron tunneling between 1D chiral quantum Hall edge states across a 1D tunnel junction for different J_0/t_0 ratios as a function of the applied bias voltage V. The case of purely elastic electron tunneling corresponds to $J_0/t_0 = 0$. Inset, top: Momentum space diagram of the chiral edge states of $LL_{1,N=1}$ and $LL_{2,M=1}$ with and without an applied bias V. Inset, bottom: Real space energy diagram in the quantum Hall regime (denoted $LL_{1,N}$ and $LL_{2,M}$, where N and M are Landau-level indices) of the two tunneling electrodes 1 and 2, respectively.

for the QH-QSL-QH tunnel junction, the entire spectral weight in the dI/dV spectrum (Fig. 3 at $V \neq 0$) arises from inelastic scattering off the spinon modes, providing a strong experimental signature.

Conclusion.—In this Letter, we have presented an extensive comparative study of tunneling signatures for various M-QSL-M junction geometries. The distinguishing feature of tunneling across a Kitaev QSL is the observation of a spectral gap and a subsequent bump in the dI/dV spectrum at small bias voltages, which is induced by inelastic spin scattering off the fractionalized spinon mode. These features are most strongly pronounced both for tunneling across planar 2D junctions [Fig. 2(b)] and for tunneling across a lateral 1D junction, with the electrodes in the quantum Hall regime (Fig. 3). Albeit we considered the exactly solvable Kitaev model for the QSL [2], the main results of our analysis can be generalized to other QSL materials as follows: For gapped QSLs with sufficiently short-ranged spin correlations, the current response [Eq. (4)] holds independently of the kind of transport setup presented in Fig. 1. In contrast, Eq. (4) applies only to the 0D STM junction in the case in which the spin correlations are algebraic [53]. This occurs, for example, in the presence of a spinon Fermi surface, which is potentially relevant for 1T-TaS_2 [54], and is left for future studies.

Using the generally applicable Eq. (2), we here discuss realistic Kitaev materials containing, weak Heisenberg interactions, in addition to Eq. (1c) as another example for QSLs with algebraic correlations [31,55]. The prefactor of these power laws is parametrically smaller than the correlations above the vison gap [Fig. 2(a)]. This results in a small low-voltage signal $dI^{\mathrm{inel}}/dV \sim V^4$ ($dI^{\mathrm{inel}}/dV \sim L^2V^3$) in STM (planar) tunneling experiments [28], while the signal substantially increases above the vison gap; cf. Figs. 2(b) and 2(d).

We differentiate this behavior from the tunneling signatures of phonons and magnons, and we conclude with a direct comparison to a 2D planar metal-antiferromagnet-metal junction. We concentrate on fluctuations about a Néel state on a hexagonal lattice [28], for which the linear magnon spectrum leads to a cubic inelastic tunneling current $I^{\mathrm{inel}} \sim V^3$. Contrary to the QSL case, this results in a smooth, quadratic contribution to the dI/dV spectrum at small bias voltages in the absence of an applied magnetic field; see [28].

It is a pleasure to thank P. P. Orth for useful discussions. E. J. K. acknowledges support by Department of Energy Basic Energy Sciences Grant No. DE-FG02- 99ER45790. M. T. R. acknowledges support from the MIT Pappalardo Fellowship. B. J. acknowledges funding from the Alexander-von-Humboldt foundation through a postdoctoral fellowship.

Note added.—Recently, we became aware of related work that focuses on the specific case of a 0D STM junction [46].

[1] P. W. Anderson, Mater. Res. Bull. **8**, 153 (1973).
[2] A. Kitaev, Ann. Phys. (Amsterdam) **321**, 2 (2006).
[3] C. Nayak, S. H. Simon, A. Stern, M. Freedman, and S. D. Sarma, Rev. Mod. Phys. **80**, 1083 (2008).
[4] G. Jackeli and G. Khaliullin, Phys. Rev. Lett. **102**, 017205 (2009).
[5] L. Savary and L. Balents, Rep. Prog. Phys. **80**, 016502 (2017).
[6] Y. Zhou, K. Kanoda, and T.-K. Ng, Rev. Mod. Phys. **89**, 025003 (2017).
[7] J. Knolle and R. Moessner, Annu. Rev. Condens. Matter Phys. **10**, 451 (2019).
[8] Y. Singh, S. Manni, J. Reuther, T. Berlijn, R. Thomale, W. Ku, S. Trebst, and P. Gegenwart, Phys. Rev. Lett. **108**, 127203 (2012).
[9] C. Balz, B. Lake, J. Reuther, H. Luetkens, R. Schönemann, T. Herrmannsdörfer, Y. Singh, A. T. M. Nazmul Islam, E. M. Wheeler, J. A. Rodriguez-Rivera, T. Guidi, G. G. Simeoni, C. Baines, and H. Ryll, Nat. Phys. **12**, 942 (2016).
[10] J. G. Cheng, G. Li, L. Balicas, J. S. Zhou, J. B. Goodenough, C. Xu, and H. D. Zhou, Phys. Rev. Lett. **107**, 197204 (2011).
[11] J. A. M. Paddison, M. Daum, Z. Dun, G. Ehlers, Y. Liu, M. B. Stone, H. Zhou, and M. Mourigal, Nat. Phys. **13**, 117 (2017).
[12] S. H. Chun, J.-W. Kim, J. Kim, H. Zheng, C. C. Stoumpos, C. Malliakas, J. Mitchell, K. Mehlawat, Y. Singh, Y. Choi *et al.*, Nat. Phys. **11**, 462 (2015).
[13] K. Kitagawa, T. Takayama, Y. Matsumoto, A. Kato, R. Takano, Y. Kishimoto, S. Bette, R. Dinnebier, G. Jackeli, and H. Takagi, Nature (London) **554**, 341 (2018).
[14] K. W. Plumb, J. P. Clancy, L. J. Sandilands, V. V. Shankar, Y. F. Hu, K. S. Burch, H.-Y. Kee, and Y.-J. Kim, Phys. Rev. B **90**, 041112(R) (2014).
[15] A. Banerjee, C. Bridges, J.-Q. Yan, A. Aczel, L. Li, M. Stone, G. Granroth, M. Lumsden, Y. Yiu, J. Knolle *et al.*, Nat. Mater. **15**, 733 (2016).
[16] A. Banerjee, J. Yan, J. Knolle, C. A. Bridges, M. B. Stone, M. D. Lumsden, D. G. Mandrus, D. A. Tennant, R. Moessner, and S. E. Nagler, Science **356**, 1055 (2017).
[17] Y. Kasahara, T. Ohnishi, Y. Mizukami, O. Tanaka, S. Ma, K. Sugii, N. Kurita, H. Tanaka, J. Nasu, Y. Motome *et al.*, Nature (London) **559**, 227 (2018).
[18] D. Aasen, R. S. K. Mong, B. M. Hunt, D. Mandrus, and J. Alicea, Phys. Rev. X **10**, 031014 (2020).
[19] D. Ghazaryan, M. T. Greenaway, Z. Wang, V. H. Guarochico-Moreira, I. J. Vera-Marun, J. Yin, Y. Liao, S. V. Morozov, O. Kristanovski, A. I. Lichtenstein, M. I. Katsnelson, F. Withers, A. Mishchenko, L. Eaves, A. K. Geim, K. S. Novoselov, and A. Misra, National electronics review **1**, 344 (2018).
[20] D. R. Klein, D. MacNeill, J. L. Lado, D. Soriano, E. Navarro-Moratalla, K. Watanabe, T. Taniguchi, S. Manni, P. Canfield, J. Fernández-Rossier, and P. Jarillo-Herrero, Science **360**, 1218 (2018).
[21] B. Zhou, Y. Wang, G. B. Osterhoudt, P. Lampen-Kelley, D. Mandrus, R. He, K. S. Burch, and E. A. Henriksen, J. Phys. Chem. Solids **128**, 291 (2019).
[22] S. Mashhadi, Y. Kim, J. Kim, D. Weber, T. Taniguchi, K. Watanabe, N. Park, B. Lotsch, J. H. Smet, M. Burghard *et al.*, Nano Lett. **19**, 4659 (2019).

[23] M. Carrega, I. J. Vera-Marun, and A. Principi, Phys. Rev. B **102**, 085412 (2020).
[24] J. Knolle, D. L. Kovrizhin, J. T. Chalker, and R. Moessner, Phys. Rev. Lett. **112**, 207203 (2014).
[25] E. V. Castro, K. S. Novoselov, S. V. Morozov, N. M. R. Peres, J. M. B. L. dos Santos, J. Nilsson, F. Guinea, A. K. Geim, and A. H. C. Neto, Phys. Rev. Lett. **99**, 216802 (2007).
[26] U. F. P. Seifert, T. Meng, and M. Vojta, Phys. Rev. B **97**, 085118 (2018).
[27] W. Choi, P. W. Klein, A. Rosch, and Y. B. Kim, Phys. Rev. B **98**, 155123 (2018).
[28] See Supplemental Material at http://link.aps.org/supplemental/10.1103/PhysRevLett.125.267206 for further information on the tunneling Hamiltonian, tunnel current derivation, Kitaev quantum spin liquid, algebraic spin correlations, and 2D antiferromagnet, which contains Refs. [2,23,24,29–36].
[29] G. Baskaran, S. Mandal, and R. Shankar, Phys. Rev. Lett. **98**, 247201 (2007).
[30] D. Boese, M. Governale, A. Rosch, and U. Zülicke, Phys. Rev. B **64**, 085315 (2001).
[31] X.-Y. Song, Y.-Z. You, and L. Balents, Phys. Rev. Lett. **117**, 037209 (2016).
[32] P. Coleman, *Introduction to Many-Body Physics* (Cambridge University Press, Cambridge, England, 2015).
[33] J. Rammer and H. Smith, Rev. Mod. Phys. **58**, 323 (1986).
[34] T. Horiguchi, J. Math. Phys. (N.Y.) **13**, 1411 (1972).
[35] A. Auerbach, *Interacting Electrons and Quantum Magnetism*, Graduate Texts in Contemporary Physics (Springer, New York, 2012).
[36] A. Auerbach and D. P. Arovas, Phys. Rev. Lett. **61**, 617 (1988).
[37] S. M. Winter, Y. Li, H. O. Jeschke, and R. Valentí, Phys. Rev. B **93**, 214431 (2016).
[38] J. Fernández-Rossier, Phys. Rev. Lett. **102**, 256802 (2009).
[39] J. Fransson, O. Eriksson, and A. V. Balatsky, Phys. Rev. B **81**, 115454 (2010).
[40] Z. Wang, S. Reschke, D. Hüvonen, S.-H. Do, K.-Y. Choi, M. Gensch, U. Nagel, T. Rõõm, and A. Loidl, Phys. Rev. Lett. **119**, 227202 (2017).
[41] A. Little, L. Wu, P. Lampen-Kelley, A. Banerjee, S. Patankar, D. Rees, C. A. Bridges, J.-Q. Yan, D. Mandrus, S. E. Nagler, and J. Orenstein, Phys. Rev. Lett. **119**, 227201 (2017).
[42] J. A. Sears, M. Songvilay, K. W. Plumb, J. P. Clancy, Y. Qiu, Y. Zhao, D. Parshall, and Y.-J. Kim, Phys. Rev. B **91**, 144420 (2015).
[43] S. Q. Murphy, J. P. Eisenstein, L. N. Pfeiffer, and K. W. West, Phys. Rev. B **52**, 14825 (1995).
[44] S. Biswas, Y. Li, S. M. Winter, J. Knolle, and R. Valentí, Phys. Rev. Lett. **123**, 237201 (2019).
[45] G. Chen and J. Lado, Phys. Rev. Research **2**, 033466 (2020).
[46] J. Feldmeier, W. Natori, M. Knap, and J. Knolle, Phys. Rev. B **102**, 134423 (2020).
[47] K. T. Law and P. A. Lee, Proc. Natl. Acad. Sci. U.S.A. **114**, 6996 (2017).
[48] M. Kratochvilova, A. D. Hillier, A. R. Wildes, L. Wang, S.-W. Cheong, and J.-G. Park, npj Quantum Mater. **2**, 42 (2017).
[49] Y. Nakata, T. Yoshizawa, K. Sugawara, Y. Umemoto, T. Takahashi, and T. Sato, ACS Appl. Nano Mater. **1**, 1456 (2018).
[50] H. Lin, W. Huang, K. Zhao, C. Lian, W. Duan, X. Chen, and S.-H. Ji, Nano Res. **11**, 4722 (2018).
[51] H. Lin, W. Huang, K. Zhao, S. Qiao, Z. Liu, J. Wu, X. Chen, and S.-H. Ji, Nano Res. **13**, 133 (2020).
[52] Y. Chen *et al.*, Nat. Phys. **16**, 218 (2020).
[53] W. Rantner and X.-G. Wen, Phys. Rev. Lett. **86**, 3871 (2001).
[54] H. Murayama, Y. Sato, T. Taniguchi, R. Kurihara, X. Z. Xing, W. Huang, S. Kasahara, Y. Kasahara, I. Kimchi, M. Yoshida, Y. Iwasa, Y. Mizukami, T. Shibauchi, M. Konczykowski, and Y. Matsuda, Phys. Rev. Research **2**, 013099 (2020).
[55] S. C. Morampudi, A. M. Turner, F. Pollmann, and F. Wilczek, Phys. Rev. Lett. **118**, 227201 (2017).